processes

MDPI

Article

Fabrication of a Charge-Conversion Polymer—Liposome for Enhancing Endosomal Escape of Drug Delivery System for α–Mangostin

Trang Thi Kieu Phan [1,2,3], Hoang Huy Nguyen [2], Xuan Thi Nguyen [2], Tung Van Nguyen [2], Linh Anh Duong [2], Linh Phuong Nguyen [4], Uyen Thu Pham [5], Hong Nhung Le [1,6], Toan Quoc Tran [1,6], Duong Thanh Nguyen [1,5,*] and Dung Thuy Nguyen Pham [7,8,*]

1 Graduate University of Science and Technology, Vietnam Academy of Science and Technology (VAST), 18 Hoang Quoc Viet St., Cau Giay Dist., Hanoi 10000, Vietnam; phantrang.2508@gmail.com (T.T.K.P.); nhungtin2k@gmail.com (H.N.L.); tranquoctoan2010@gmail.com (T.Q.T.)
2 Institute of Genome Research, Vietnam Academy of Science and Technology (VAST), 18 Hoang Quoc Viet St., Cau Giay Dist., Hanoi 10000, Vietnam; myphamvemb@gmail.com (H.H.N.); dtnlab.vast@gmail.com (X.T.N.); tungnv@igr.ac.vn (T.V.N.); dalinh@igr.ac.vn (L.A.D.)
3 Vinmec Research Institute of Stem Cell and Gene Technology, Hanoi 10000, Vietnam
4 School of Preventive Medicine and Public Health, Hanoi Medical University, 1 Ton That Tung St., Dong Da Dist., Hanoi 10000, Vietnam; nplinh239@gmail.com
5 Institute for Tropical Technology, Vietnam Academy of Science and Technology (VAST), 18 Hoang Quoc Viet St., Cau Giay Dist., Hanoi 10000, Vietnam; phamuyenpjj@gmail.com
6 Institute of Natural Products Chemistry, Vietnam Academy of Science and Technology (VAST), 18 Hoang Quoc Viet St., Cau Giay Dist., Hanoi 10000, Vietnam
7 NTT Institute of Applied Technology and Sustainable Development, Nguyen Tat Thanh University, Ho Chi Minh City 70000, Vietnam
8 Faculty of Environmental and Food Engineering, Nguyen Tat Thanh University, Ho Chi Minh City 70000, Vietnam
* Correspondence: ntduong182@gmail.com (D.T.N.); pntthuydung@ntt.edu.vn or pntdung@ntt.edu.vn (D.T.N.P.)

check for updates

Citation: Phan, T.T.K.; Nguyen, H.H.; Nguyen, X.T.; Van Nguyen, T.; Duong, L.A.; Nguyen, L.P.; Pham, U.T.; Le, H.N.; Tran, T.Q.; Nguyen, D.T.; et al. Fabrication of a Charge-Conversion Polymer—Liposome for Enhancing Endosomal Escape of Drug Delivery System for α–Mangostin. *Processes* **2023**, *11*, 2344. https://doi.org/10.3390/pr11082344

Academic Editor: Roberta Campardelli

Received: 5 June 2023
Revised: 26 June 2023
Accepted: 12 July 2023
Published: 4 August 2023

Abstract: α–Mangostin, which is a natural xanthone compound, inhibits the metastasis and survival of various cancer cell types. However, its therapeutic effectiveness is limited by low water solubility and very poor absorption. There are several studies that developed the drug delivery system for α–mangostin, but they are still a remaining challenge. Drug delivery techniques are severely hampered by the breakdown of nanoparticles inside endosomes. The abrasive chemical environment in these compartments causes both the nanoparticles and the encapsulated α–mangostin to degrade throughout the course of the voyage. Intracellular defenses against external materials refer to this collective mechanism. A pH-responsive liposome named PAsp(DET-Cit)–Toc, made of lipids and a charge-conversion polymer (CCP), has been created for the targeted transport of α–mangostin in order to avoid this deteriorative outcome. The average hydrodynamic size of CCP–liposome particles is 98.59 ± 5.1 nm with a PDI of 0.098 ± 0.02 and a negative zeta potential of 22.31 ± 2.4 mV. TEM showed the shape of the spherical CCP–liposomes. α–Mangostin is successfully captured inside CCP–liposome and the loading yield reached the highest encapsulation efficiency of 83% with 150 μg/mL of α–mangostin. In the acidic condition of pH 5.0, an initial burst of α–mangostin reached 50% after 6 h in buffer solution. CCP–liposomes could escape from endosomes even after 3 h, and almost 80% of CCP–liposomes escaped after 24 h. The cell ability of α–mangostin-loaded-CCP–liposome incubated in buffer solutions of 5.0 decreased significantly and was close to free α–mangostin. Our data proved that α–mangostin-loaded CCP–liposome delivered more effectively α–mangostin into cells and prevented the degradation of α–mangostin inside cells, especially endosomal degradation.

Keywords: liposome; charge-conversion polymer; α–mangostin; DDS

1. Introduction

The application of natural based-compound products is a promising therapy for disease treatment, especially cancer. α–Mangostin is known as a xanthone derivate isolated from the pericarp of the mangosteen fruit of *Garcinia mangostana* Linn. Scientists' interest in this compound has grown as a result of its potent anticancer properties [1–4]. α–Mangostin has proved effective in several cancer types, such as human prostate carcinoma [5], lung adenocarcinoma cells [6,7], and breast adenocarcinoma [2,8]. Despite its potential biological and pharmacological capabilities in cancer treatment, α–mangostin has certain limitations, including weak water solubility, which results in relatively poor absorption, limiting its anticancer effects [9,10]. In order to overcome this limitation, nanoparticles, or nanomaterials, were developed as a drug delivery system to reach high water solubility and biodistribution [10–12]. The diversity of nanoformulation drug delivery systems, such as nanomicelles, liposomes, and solid lipid nanoparticles, have been designed to ameliorate the limitation of α–mangostin and increase its delivery to achieve better therapeutic outcomes [10].

Liposomes are a revolutionary drug delivery system in several biomedical fields [13,14]. Liposomes exhibit various distinct benefits, including high biocompatibility, bioavailability, and degradability by stabilizing acquired molecules, overcoming hurdles to cell/tissue absorption, and enhancing drug/compound distribution to target areas in the body [15–17]. Therefore, liposomes can support protecting compounds from early inactivation, oxidation in the bloodstream, and upgrade aggregation in the tumor [13,18,19]. Recently, we have developed a liposome system that encapsulates α–mangostin and is capable of releasing α–mangostin to HepG2 cells [20]. Furthermore, the FDA has authorized various liposomal medications, including Myocet, Doxil, and Marqibo [21]. However, liposomes also encounter defense systems within cells with aims to recognize, neutralize and eliminate the invading foreign substances [13]. These barriers include the reticuloendothelial system, opsonization, and immunogenicity.

The liposome has a lipid bilayer structure, so it is easy to absorb into the membrane of cells and results in the release of the active compound into the extracellular fluid. In addition, the liposomes can interact with cells via receptor-mediated endocytosis, but it only permits vesicles of a maximum diameter of 150 nm, and liposomal content has the ability to endure the acidic environment of lysosomes. In addition, it is difficult for liposomes to escape endocytosis inside cells, in which endosomes fuse with liposomes leading to the degradation of liposomes via a low pH and the release of drugs [22–24]. For liposomes, early endosomes serve as a pivotal checkpoint that determines whether they will be recycled, excreted, or degraded. Liposomes have the potential to either evade the early endosome and progress further, leading to the formation of late endosomes, or they can become entrapped within the early endosome and subsequently merge with lysosomes to form endo-lysosome vesicles, resulting in their degradation [25]. As a result, in order to sustain their therapeutic effectiveness, drug-based liposome delivery systems must resist rapid breakdown and escape early endosomes.

Numerous studies have developed smart polymers that are responsive to environmental factors, including pH, temperature, and ionic strength. Additionally, pH-sensitive polymers have advanced to the point where they may include acetal, ester, and hydrazone into their acid-labile linkage, allowing the medication to be released from the endosome [26–28]. However, because these polymers have a positive charge, they are easily attached to molecules in blood arteries and are detected by the reticuloendothelial system throughout their circulation in the blood. Therefore, charge-conversion polymer (CCP) needs to possess negative charges at neutral pH conditions (blood or cytoplasm), and when entrapped by an endosome, CCP absorbed protons (H^+) in the endosome environment to neutralize its negative charge at acidic pH (endosome or secondary lysosomes) result in endosome swell and burst [29,30]. Finally, the active compound will be released from the endosome.

In this research, we designed a drug delivery system including two main components (1) liposomes are composed of phospholipids and cholesterol as carriers; (2) CCP–Toc: a charge-conversion polymer, which has Toc side chains to bind to liposomes, this CCP–Toc supports liposome escape from endosomal degradation (Figure 1). This system applies to improve the limitation and delivery α–mangostin and enhance its therapeutic performance for cancer treatment.

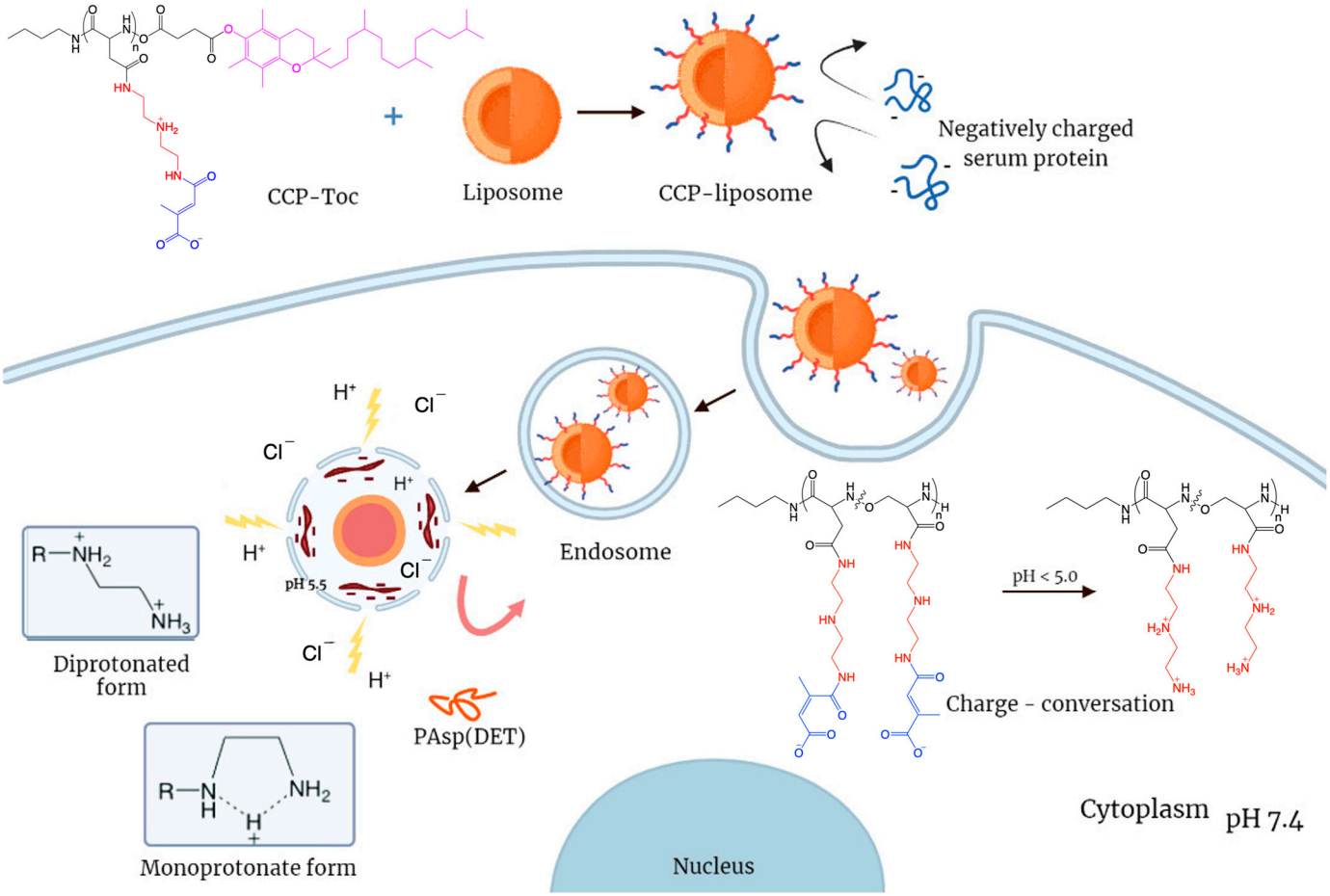

Figure 1. Schematic of endosomal escape mechanism of a charge-conversion polymer modified liposome.

2. Materials and Methods

2.1. Materials

α–Mangostin, *N*-hydroxysuccinimide (NHS), *N*,*N*-dimethylformamide (DMF), dichloromethane (DCM), methanol (MeOH), diethylenetriamine (DET), and *N*-methyl-2-pyrrolidone (NMP) were supplied by Wako Pure Chemical Industries, Ltd. (Osaka, Japan). The 1-ethyl-3-(3-dimethylaminopropyl)-carbodiimide hydrochloride (EDC) was acquired from Sigma-Aldrich (Merck, Germany). Fuchs' approach was used to generate benzyl-L-aspartate *N*-carboxy-anhydride (BLA–NCA). [31]. Polycarbonate membrane filters were acquired from Whatman Inc. (Clifton, NJ, USA). Dioleoyl, palmitoyl-oleoyl, and dimyristoyl phosphatidyl ethanolamines (DOPE, POPE, and DMPE) were from Avanti-Polar Lipids, Inc. (Alabaster, AL, USA). Carboxyfluorescein (CF), triton X-100, alpha-tocopheryl succinate (α–TOS), chloroform, and phosphate-buffered saline (PBS) were obtained from Sigma-Aldrich. All other chemicals used were of analytical grade. The laser scanning confocal microscope TCS SP5 AOBS was acquired from Leica (Wetzlar, Germany).

2.2. Methods

2.2.1. Synthesis of Charge–Conversion Polymer PAsp(DET-Cit)–Toc

- Synthesis of *N*-Succinimidyl Tocopheryl Succinate

N-succinimidyl tocopheryl succinate was synthesized from tocopheryl succinate and *N*-hydroxysuccinimide with the presence of wet suck catalyst (WSC). Tocopheryl succinate (1.74 g, 3.28 mmol), NHS (0.38 g, 3.28 mmol), and EDC (0.64 g, 3.28 mmol) were dissolved in 50 mL DCM. The mixture was agitated at ambient temperature for a duration of 48 h under an argon atmosphere. Upon the completion of the reaction, the solution was rinsed with 100 mL of distilled water before the organic phase was extracted. With DCM, the aqueous phase was back-extracted twice in 50 mL each. After filtering, the mixed organic phase was dried with $MgSO_4$. The substance was obtained as a yellow gel (1.9 g, 91% of the product) by isolating the product by solvent evaporation at decreased pressure. The conversion rate of carboxyl group in tocopheryl succinate was determined to be 100% from the peak intensity ratio of the ethylene groups in succinimide ring (–CH_2CH_2–, δ = 2.8 ppm) and methyl groups binding with pheryl of tocopherol (($(CH_3)_3C_6$–, δ = 1.9, 2.0, 2.1 ppm) in ^{1}H NMR spectrum (7.5 mg/mL, 25 °C).

- Synthesis of PBLA

n-Butylamine was used to ring-open polymerize the BLA–NCA, resulting in the synthesis of poly(β-benzyl L-aspartate) (PBLA). BLA–NCA (2.49 g, 10 mmol) was collected and weighted inside an argon bag to prevent any contact with water and then dissolved in the mixture of DMF (10.0 mL) and CH_2Cl_2 (100 mL) at 40 °C. DCM was used to dilute *n*-butylamine (14.6 mg, 200 mmol) before introducing to the BLA–NCA solution. The polymerization was reacted for 48 h at 40 °C under argon. IR measurements were used to determine the end of polymerization.

The PBLA product was three times precipitated in ether (3 L) for purification. The resultant precipitate underwent filtering before being freeze-dried using benzene as the solvent. BLA unit has a polymerization degree of 20 based on ^{1}H NMR spectroscopy by comparing the ratio of the proton in methyl group ($CH_3CH_2CH_2CH_2$–, δ = 0.8 ppm) and the proton in benzyl group ($C_6H_5CH_2$–, δ = 5.1 and 7.3 ppm) or the proton in α–CH group (COCHNH-, δ = 4.7 ppm). The monodispersity with M_w/M_n = 1.1 was confirmed by GPC measurement.

Similarly, PBLA polymers with various degrees of polymerization (DP = 32, 73, 106) were synthesized and characterized.

- Synthesis of PBLA–Toc

The conjugation of hydrophobic group α–tocopherol to the end chain of a single platformed PBLA was prepared through the reaction of PBLA and *N*-hydroxysuccinimide—activated acid of tocopheryl succinate. Lyophilized PBLA (DP = 20; m = 150 mg, 0.0375 mmol) was dissolved in 10 mL DCM. The solution was then added to 50-folds of *N*-succinimidyl tocopheryl succinate (1.2 mg, 1.875 mmol) in 7 mL DCM. The solution was agitated at ambient temperature for a duration of 48 h under argon pressure. The product was collected by precipitation in 300 mL diethyl ether, followed by lyophilization to give white powder product (167.2 mg, 98%). The conversion rate of amine group in PBLA was calculated to be % from the peak intensity ratio of the methyl groups (CH_3CH–, δ = 1.8–2.0 ppm) and in α–CH group (–COCHNH–, δ = 4.7 ppm) in ^{1}H NMR spectrum (7.5 mg/mL, 80 °C). The monodispersity with M_w/M_n = 1.1 was confirmed by GPC measurement.

Similarly, PBLA–Toc polymers with various degrees of polymerization (DP = 32, 73, 106) were synthesized and characterized.

- Synthesis of PAsp(DET)–Toc

The aminolysis reaction of PBLA with DET under moderate anhydrous conditions was used to introduce amino groups into the PBLA side chain. Lyophilized PBLA-Toc (DP = 20, m = 150 mg, 0.65 mmol BLA) was dissolved in NMP (10 mL) (solution A). DET (V = 3.5 mL, 32.5 mmol, or 50 folds of BLA) was diluted in NMP (5 mL) (solution B). Both solutions

were cooled down to 4 °C before adding dropwise solution A into solution B. The reaction mixture was agitated at 4 °C for 4 h. The resulting solution was then neutralized gradually by 0.5 N HCl in a salt-ice system to control temperature below 2 °C. The neutralized solution was dialyzed in 0.01 N hydrochloric acid solution (4 times) and distilled water (1 time). The white powder, PAsp(DET)–Toc, was obtained as hydrochloric salt after lyophilization (mg, % yield). No benzyl peak was seen in ^{1}H NMR spectrum. The quantitative conversion of PBLA to PAsp(DET) by the aminolysis reaction was verified by ^{1}H NMR from the peak intensity ratio of the protons of the α–CH group (–COCHNH–, δ = 4.7 ppm) to the ethylene groups in the 1,2-diaminoethane (PAsp(DET): $H_2N(CH_2)_2NH(CH_2)_2NH$–, δ = 3.2–3.6 ppm) settled at the side chain. Similarly, PAsp(DET)–Toc polymers with various degrees of polymerization (DP = 32, 73, 106) were synthesized and characterized.

- Synthesis of PAsp(DET-Cit)–Toc

PBLA (DP = 20, m = 50 mg, 0.22 mmol Asp (DET)) was dissolved in 450 mL 0.5 M $NaHCO_3$ buffer (pH = 8.92). The solution was then added cis-Aconitic anhydride (m = 1.75 g, 11.1 mmol or 50 folds Asp(DET)) gradually. The reaction mixture was stirred at 4 °C for 4 h. The final solution was purified 3 times with distilled water through Amicon Ultra filler units (MWCO = 3000; Millipore, Billerica, MA, USA). The product was obtained after lyophilization as a white powder (67 mg, 78%). The conversion yield was calculated from the peak intensity ratio of the methyl groups (–OCOC(CH_3)CH–, δ = ppm) and in α–CH group (–COCHNH–, δ = 4.7 ppm) in ^{1}H NMR spectrum (7.5 mg/mL, 80 °C).

Similarly, PAsp(DET-Cit)–Toc polymers with various degrees of polymerization (DP = 32, 73, 106) were synthesized and characterized.

2.2.2. Preparation of Liposome

The film hydration process and subsequent extrusion were used for preparation of liposomes. In total, 0.3 mL of 0.01 M PAsp(DET-Cit)–Toc solution, 2.5 mL of 0.025 M DOPC stock solution, and 1 mL of 0.02 M -Mangostin stock solution were mixed together in an Eppendorf tube using chloroform as the solvent. The mixture was vortexed for 2 min before being transferred to a flask with a flat bottom. Subsequently, the solvents were extracted from the mixture using a Rotavapor R-100 at 40 °C, 250 mBar, and a rotational speed of 2. In total, 3 mL distilled water was added to the mixture and sonicated at 40 °C for 30 s. The opaque suspension containing α–Mangostin-loaded-CCP–liposome and unencapsulated α–Mangostin was formed and dialyzed (MWCO = 14,000 Da, 2 L dH_2O, 24 h) to remove unencapsulated α–Mangostin. Liposomes were extruded through 100 nm size polycarbonate membrane filters (30 times) (Whatman Inc., Clifton, NJ, USA) to create vesicles with a comparatively consistent mean size. The mixture was pre-equilibrated in phosphate-buffered saline (pH 7.4) before detaching non-encapsulated α–mangostin by size exclusion chromatography (PD10 Sephadex® G- 25 M column). Blank liposomes (without α–mangostin and CCP) and CCP–liposomes (without α–mangostin) are synthesized with the same process without adding materials.

2.2.3. Measurement of Dynamic Light Scattering (DLS)

To measure the size, the DLS instrument (Horiba, Japan) employs the principle of light scattering by particles in solution, allowing for the calculation of the hydrodynamic diameter of CCP–liposomes that were maintained at ambient temperature. Furthermore, the zeta potential, which reflects the surface charge and stability of the liposomes, was assessed using the electrophoretic mobility of the particles in an electric field.

2.2.4. Drug Loading and Encapsulation Efficiency

The EE% and DL% were measured according to the previously described procedure [32]. Briefly, after water was removed, the CCP–liposome film was dissolved in 3.5 mL $CHCl_3$/MeOH (1:3, v/v) and subjected to bath sonication for 2 min. Then, the resultant solution was diluted with 2.9 mL of $CHCl_3$/MeOH (1:3, v/v) and measured absorbance at

243 nm using UV-Vis spectrophotometer (Hitachi U-2900, Tokyo, Japan) in comparison to a reference solution of $CHCl_3$/ MeOH (1:3, v/v).

2.2.5. Drug Release

α–Mangostin release from CCP-liposome behavior was determined by dialysis method. α–angostin-loaded-CCP–liposome was first dissolved in dd-H_2O and transferred to dialysis tubing (MWCO = 1400 Da), and immersed in phosphate buffer saline (0.1 M, pH 7.4) and acetate buffer (0.1 M, pH 5.0, 6.0), at a speed of 110 rpm, 37 °C. Each condition of samples was examined in triplicate. For time intervals, the determined volume of release medium was replaced with the same volume of the fresh buffer solution. The amount of α–Mangostin release from CCP–liposome was calculated by measuring the absorbed intensity at 480 nm using a UV spectrophotometer.

2.2.6. In-Vitro Uptake of CCP–Liposome by HepG2 Cells

Human hepatocellular carcinoma (Hep-G2) cells (American Type Culture Collection, Manassas, VA, USA) was cultured in DMEM containing 100 µg/mL streptomycin sulfate, 100 units/mL penicillin G, and 10% FBS in humidified atmosphere of 95% air and 5% CO_2 at 37 °C. Further experiments were conducted using exponentially growing cells.

HepG2 cells were plated onto a 6-well plate (1×10^6 per well) containing 1 mL of DMEM for a flow cytometry study. The cells were allowed to attach to the plate under incubation at 5% CO_2 and 37 °C for 24 h. Then, CFPE-labeled liposomes at a final concentration of 2 g/mL were added to the cells, whereas the control group received liposome-free culture medium. After a 6-h incubation period, the cells were washed three times with cold PBS, trypsinized, and resuspended in 0.3 mL of PBS. The cell fluorescence intensity was measured by using Cytomics FC 500 cytometer (Beckman Coulter, Brea, CA, USA) with excitation and emission wavelengths of 495 nm and 515 nm, respectively.

2.2.7. Confocal Laser Scanning Microscopy (CLSM)

Each of the wells of a 6-well plate was plated with HepG2 cells (1×10^5 cells) on a cover slip. After 24 h, CFPE-labeled liposomes were added to each well and incubated for another 6 h. At 30 min before the conclusion of the incubation, Lysotracker Red with an excitation peak at 573 nm and an emission peak at 592 nm was applied to each well. The cells were then rinsed three times with cold PBS before being fixed with 4% paraformaldehyde at room temperature for 15 min, followed by nuclei staining with Hofor for 5 min. The cells were examined using TCS SP5 AOBS confocal microscopy system (Leica, Germany).

2.2.8. Cytotoxicity Assay

HepG2 cells were cultured overnight at 37 °C in a 5% CO_2 environment in 96-well plates with DMEM. The cytotoxicity of free drug, blank CCP–liposomes, and drug-loaded CCP–liposomes was assessed using an MTT test (Sigma-Aldrich, St. Louis, MO, USA). The absorbance at 570 nm of each well was measured using a Spectramax M5 Microtiter Plate Luminometer (Molecular Devices, San Jose, CA, USA).

2.2.9. Endosomal Escape Property

HepG2 cells were immediately given CCP–liposomes and incubated in 5% CO_2 at 37 °C. Following Triton X treatment and 4% formaldehyde fixation, cells were stained for 30 min using Cyanine 3, which has a peak excitation wavelength at 555 nm and a peak emission wavelength at 569 nm, as well as Hoechst 33342 with an excitation peak at 352 nm and an emission peak at 454 nm. For fluorescence imaging, a Nikon A1 confocal laser-scanning microscope was employed. HepG2 was exposed to 105 cells/mL and suppressed for 1 h in order to conduct tests on the mechanisms behind cell uptake. For 30 min, Cyanine 3 and Hoechst 33342 were used to pre-treat the cells. Before repairing, Lysotracker Green with excitation/emission maxima of 504/511 nm was employed in the endosomal escape experiment. Using the colocalization threshold and coloc2 plugin in

ImageJ program, the level of colocalization was measured based on Pearson's correlation coefficient (R).

2.2.10. Statistical Analysis

The data were analyzed using one-way ANOVA and StatPlus: mac LE software version v7.3.31 (Analystsoft Inc., Walnut, CA, USA), with * $p < 0.05$ considered as statistical difference.

3. Results and Discussion

3.1. Synthesis of Charge-Conversion Polymer PAsp(DET-Cit)–Toc

3.1.1. Synthesis of *N*-Succinimidyl Tocopheryl Succinate

The charge-conversion polymer Pasp(DET-Cit)–Toc was designed and synthesized following Scheme 1. First, *N*-succinimidyl tocopheryl succinate was synthesized by coupling tocopheryl succinate and NHS and with the presence of WSC (EDC) in the DCM (Scheme 1). The product was confirmed by ^{1}H NMR measurement in chloroform—d_3 (CD_3Cl) at 25 °C (Figure 2A). The peak of the ethylene group of the succinimide ring appeared clearly in the ^{1}H NMR spectrum. Comparing the proton ratio of ethylene protons in the succinimide ring and methyl protons bonding with the pheryl group of tocopherol confirmed the conversion rate of the carboxyl group in tocopheryl succinate to be 100%.

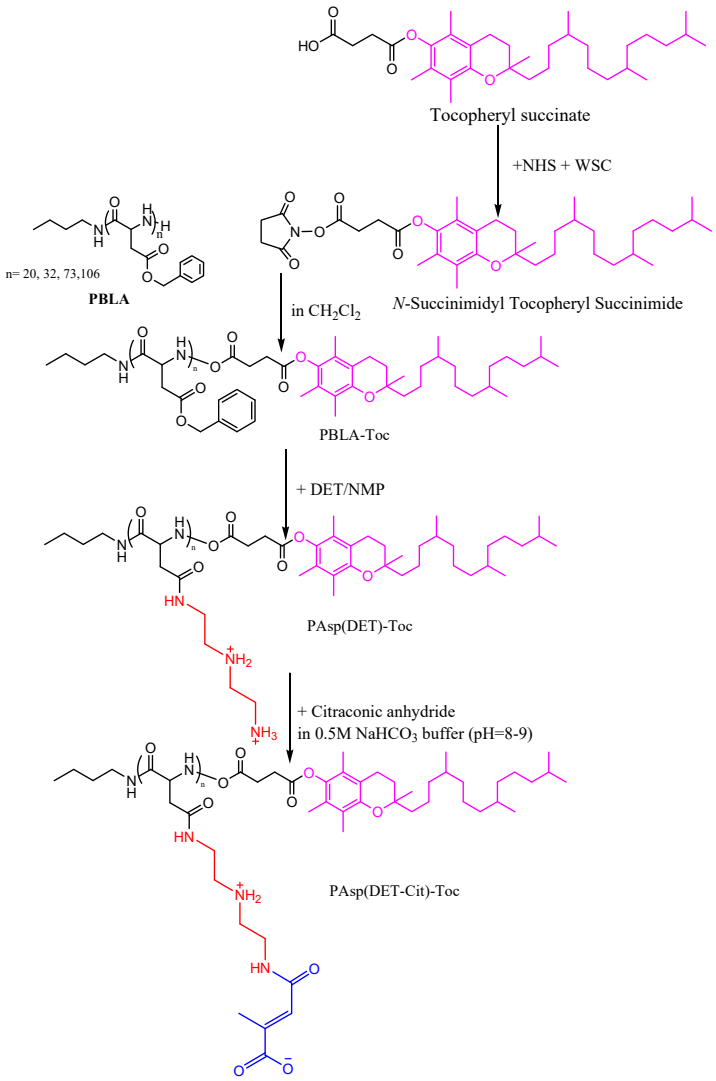

Scheme 1. Procedures of PAsp(DET-Cit)–Toc synthesis.

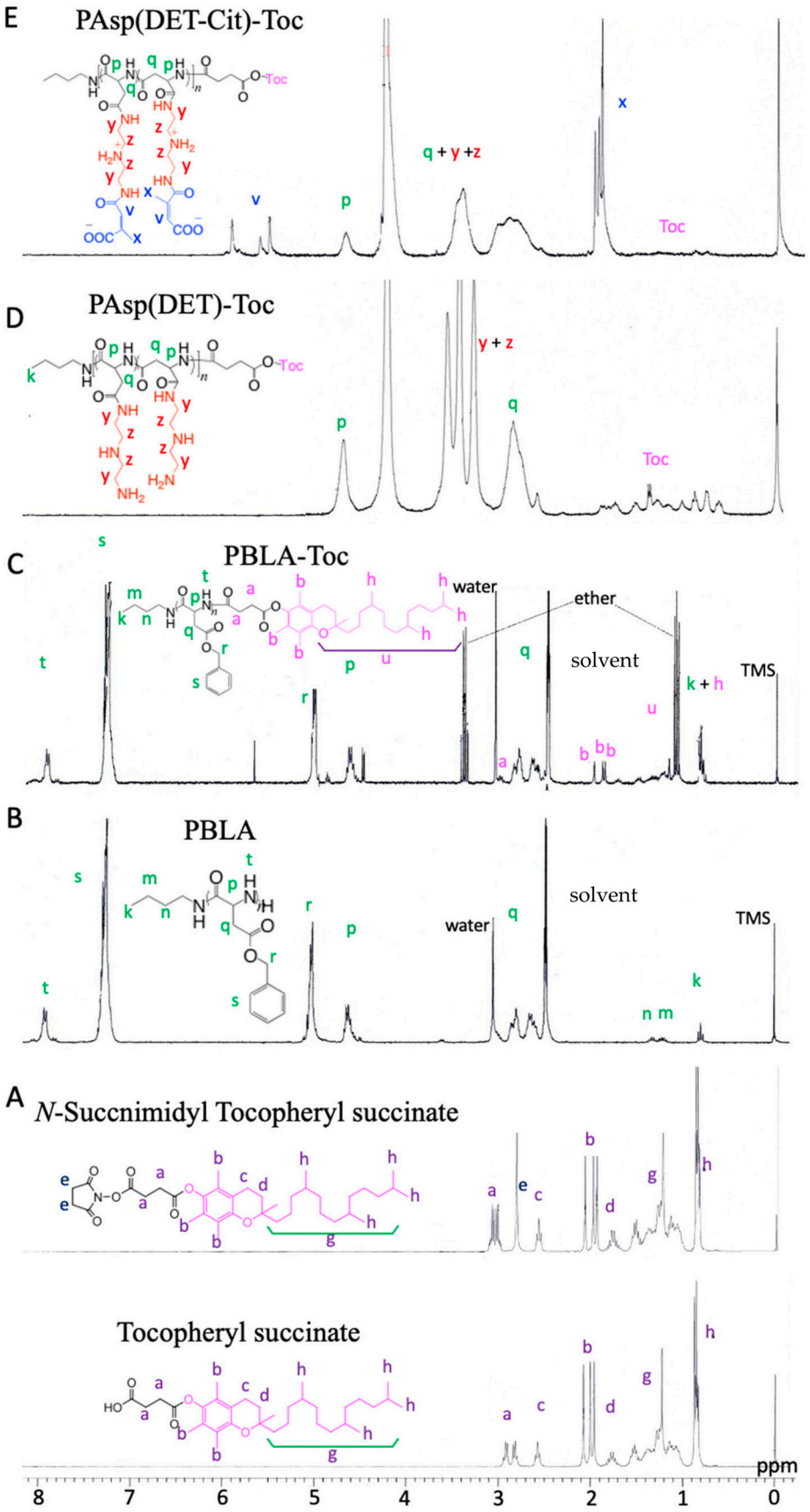

Figure 2. The ^{1}H NMR spectra of (**A**) tocopheryl succinate and *N*-succinimidyl tocopheryl succinate (**B**) PBLA (**C**) PBLA–Toc (**D**) PAsp(DET)–Toc and (**E**) PAsp(DET-Cit)–Toc.

3.1.2. Synthesis of PBLA

Afterward, PBLA was synthesized by ring-opening polymerization of BLA–NCA triggered by the NH_2 group of n-butylamine (Scheme 1). The polymerization was confirmed by monitoring specific peaks of NCA disappeared (1850 cm^{-1}: C=O asymmetric stretching; 1780 cm^{-1}: C=O symmetric stretching; 910 cm^{-1}: C=O deformation) (Figure 2B). The polymerization degree of PBLA segment in PBLA block copolymers was estimated as 20 by ^{1}H-NMR measurements in DMSO-d_6 at 80 °C comparing the proton ratios of the methyl protons in butyl group ($CH_3CH_2CH_2CH_2$–, δ = 0.8 ppm) and the α–CH group (COCHNH–, δ = 4.7 ppm) (Figure 2B). The monodispersity for PBLA (DP = 20) was confirmed by NMP-GPC measurement (M_w/M_n = 1.19).

3.1.3. Synthesis of PBLA–Toc

Similarly, PBLA–Toc polymers with different degrees of polymerization (DP = 32, 73, 106) underwent characterization through ^{1}H-NMR measurements and NMP-GPC (Figure 3C). The amide bond formed between *N*-succinimidyl tocopheryl succinate and the amine group at the end chain of PBLA was used to produce PBLA–Toc (Scheme 1). The product was confirmed by the ^{1}H NMR spectrum. The peaks of the tocopheryl group in PBLA-Toc appeared at 0.8–2.1 ppm. The conversion of distal end amino group NH_2 of the PBLA chain was determined by calculating the relative molar ratio of methyl protons of tocopheryl succinate ($((CH_3)_3C_6$–, δ = 1.8–2.0 ppm) to α–CH group (–COCHNH–, δ = 4.7 ppm) in ^{1}H NMR spectrum (Figure 3C).

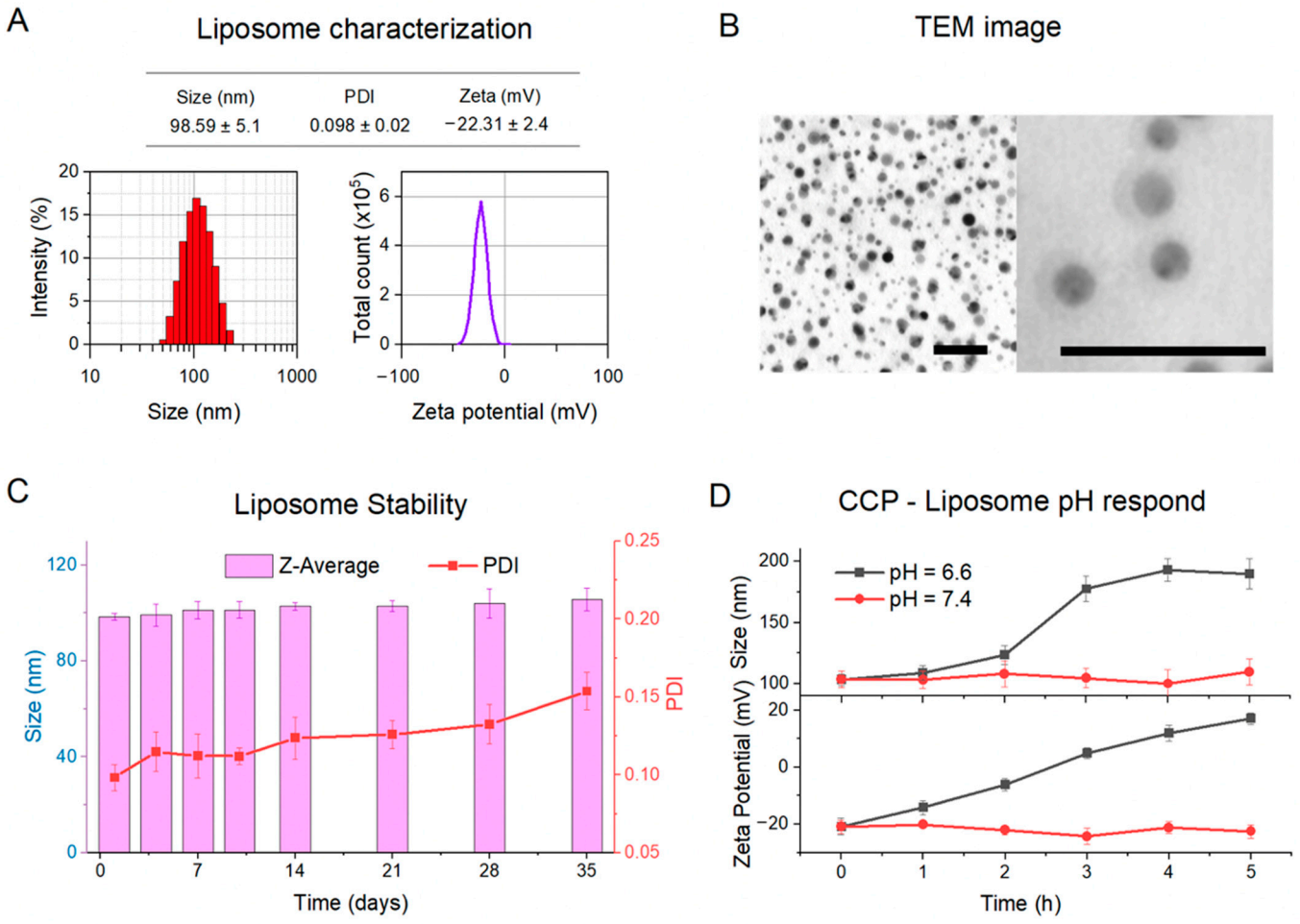

Figure 3. Characterizations of CCP–liposome. (**A**) The surface charge distribution is indicated by the distribution of hydrodynamic size and zeta potential of CCP–liposomes. (**B**) TEM images of

CCP–liposomes taken at various magnifications. Scale bars indicate 500 nm. (**C**) Assessment of CCP–liposome stability over a 35-day period by monitoring changes in hydrodynamic size and polydispersity index (PDI) (**D**) Examination of size and zeta potential changes in CCP–liposomes across different pH solutions over a 5-h timeframe. Data are presented as the mean ± SD (n = 3). The variation in the zeta potential value depicted the charge-conversion characteristic of the CCP–liposome, as demonstrated in (**D**). The CCP–liposome complex exhibited a consistent zeta potential of approximately −20 mV at pH 7.4. However, at pH 6.6, the zeta potential progressively transitioned from negative to positive as a result of the degradation of the cis-aconitic amide group in the polymer. The zeta potential value reached 0 mV after 2 h incubation at pH 6.6 and changed to a positive value. It showed no change of zeta potential in pH 7.4.

The PBLA polymers (DP = 32, 73, 106) reacted with *N*-succinimidyl tocopheryl succinate in the same condition as PBLA DP = 20. Comparing the conjugation of tocopherol to the distal end of PBLA with different degrees of polymerization, the conversion rate was decreased due to the longer polymer chain. Because of the random coil structure, the distal amine group of the polymers with higher DP is difficult to interact with *N*-hydroxysuccinate activated by tocopheryl succinate. A longer reaction time is required for amide bond formation of PBLA and *N*-succinimidyl tocopheryl succinate. In addition, The NMP-GPC measurement confirmed the conjugation of tocopherol to the PBLA polymer chain did not affect the polymer structure. The increase in polymer weight was reasonable due to the addition of the tocopherol group to the distal end of PBLA.

3.1.4. Synthesis of PAsp(DET)–Toc

PBLA–Toc was aminolized by diethylenetriamine (DET) in the NMP under a mind condition. The reaction was described in Scheme 1. A range of cationic side chains derived from a single platformed PBLA was synthesized through a quantitative aminolysis reaction [33–35]. The process begins with the activation of the nitrogen atom in the main chain via the interaction of an amine as a weak base, in which hydrogen bonds with the proton of the amide group. Subsequently, the activated nitrogen attacks the carbon atom of the carbonyl group in the side chain, resulting in the formation of the succinimidyl ring. Then, an amine molecule attacks one of the two carbonyl groups inside the succinimidyl ring, resulting in the effective conversion of the ring into an *N*-substituted poly(aspartamide) derivative [36]. Therefore, a quantitative aminolysis reaction does not affect an amide bond through PBLA and tocopheryl succinate. This result was also confirmed by the ^{1}H NMR spectrum (Figure 2D). The ^{1}H NMR spectra of PAsp(DET)–Toc showed the appearance of the ethylene groups in the 1,2-diaminoethane (PAsp(DET): $H_2N(CH_2)_2NH(CH_2)_2NH$–, δ = 3.2–3.6 ppm), while the peaks from benzyl disappeared demonstrating substation with DET proceeds.

3.1.5. Synthesis of PAsp(DET-Cit)–Toc

Pasp(DET-Cit)–Toc was created by reacting PAsp(DET)–Toc with Citraconic anhydride in 0.5 M $NaHCO_3$ buffer (pH = 8–9) (Scheme 1). The product was confirmed by the ^{1}H NMR spectrum and characterized by HPLC (Water GPC). The methyl group (CH_3C–, δ = 1.9 ppm) and the methine group (–CH–, δ = 5.5–5.9 ppm) of citraconic appeared clearly in the ^{1}H NMR spectrum (Figure 2E). The group peaks of methine group were explained by the structure of the double bond (C=C) and the binding of different CO groups to the DET. The conversion rate of PAsp(DET-Cit)–Toc was determined through the comparison of the proton intensity of methine protons of citraconic with the α–CH group of the polymer chain. The production has also checked the degradation by HPLC.

3.2. Physical Characterizations of CCP–Liposome

The size, surface properties, and morphological features of the CCP–liposome were analyzed by DLS and TEM. DLS measurements revealed that the average hydrodynamic size of CCP–liposome particles was 98.59 ± 5.1 nm, with a polydispersity index of 0.098 ± 0.02

and a negative zeta potential of 22.31 ± 2.4 mV. (Figure 3A). The spherical CCP–liposomes' shape has been observed using TEM (Figure 3B). To confirm its colloidal stability, CCP–liposome underwent a 35-day hydrodynamic size and PDI analysis (Figure 3C). The liposome's stability was demonstrated by the nominal changes in hydrodynamic size and PDI during the course of 35 days of observation.

In addition, the dramatic size change of the CCP–liposome complex also was induced by the charge conversion. As results showed in Figure 3D, at pH 7.4, the CCP–liposome complex remained around 100 nm in size. At pH 6.6, however, there was an instantaneous rise in their size. Large aggregates with diameters of almost 200 nm have developed. The aggravation was most likely caused by a decrease in repulsive forces as a result of partial charge neutralization after 1 h of incubation and total neutralization after 2 h at an acidic pH of 6.6.

3.3. The Release Rate and Encapsulation Efficiency of CCP–Liposome

The drug loading yield reached the highest capacity of 17.4% with 150 µg/mL of α–mangostin (Figure 4A). When the concentration of α–mangostin increased to 200 µg/mL and 300 µg/mL, the drug loading capacity decreased to 14.57% and 14%, respectively. Moreover, with the α–mangostin concentration of 150 µg/mL, the encapsulation efficiency is nearly 90%.

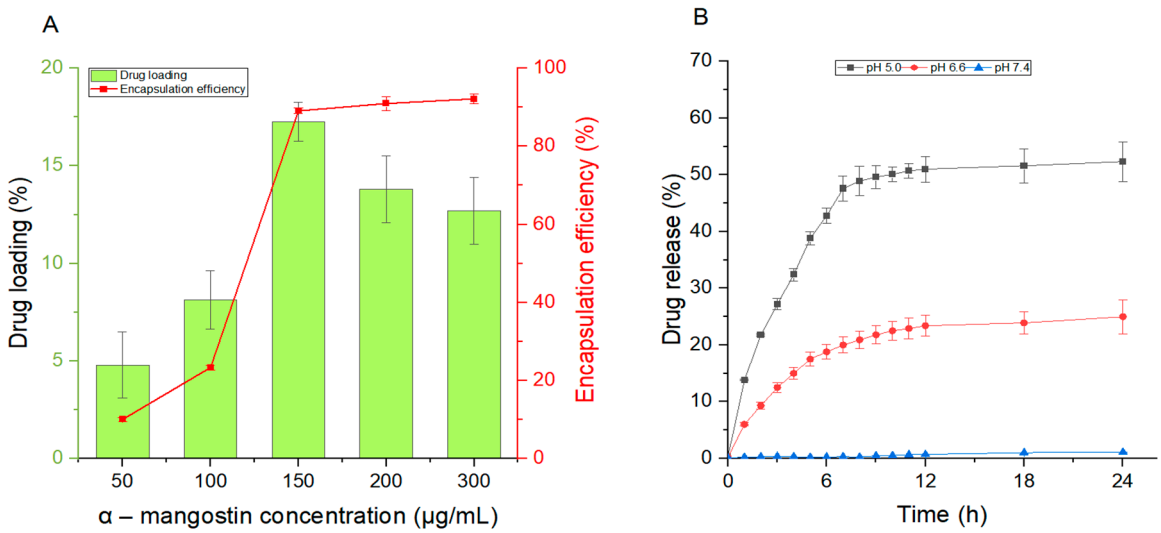

Figure 4. Characterizations of α–mangostin CCP–liposome. (**A**) Drug loading and encapsulation efficiency; (**B**) Release profile of α–mangostin CCP–liposome. Data are presented as the mean ± SD (n = 3).

In terms of release profile, drug release at pH 5.0 was substantially quicker than at between pH 6.6 and 7.4, which was consistent with the qualitative results. The α–mangostin release was slower at pH 7.4, and the drug release quantity was virtually 0% in 24 h, indicating that the drug may be well encapsulated in the CCP–liposome, which is beneficial for CCP–liposome circulation in vivo and also reduces cytotoxicity. In an acidic pH 5.0 solution, there was an early burst of α–mangostin that reached 50% after 12 h and then remained stable for another 24 h (Figure 4B). It is most likely pH hydrolysis of Cit-Toc at pH 5.0, resulting in fast drug diffusion via swelling liposome particles.

3.4. Endosome Escape of CCP–Liposome

Rapid lysosomal drug release is indispensable, while nanoparticles are eventually entrapped inside the lysosome after endocytosis. Therefore, the intracellular uptake of nanoparticles and drug release were investigated. As shown in Figure 5A, both liposomes and CCP–liposomes were able to penetrate into cells. CCP–liposomes demonstrated a

much greater cellular absorption than liposome particles, indicating the presence of CCP on the surface of more sensitive liposomes. Furthermore, a quantitative examination of flow cytometry data revealed the same result (Figure 5B). The confocal images also indicated CCP–liposome and liposome cellular trafficking. After 6 h of incubation, CCP–liposome fluorescence (red) was clearly visible in HepG2 cells, whereas liposome fluorescence was haphazardly spread over the cell membrane (Figure 5C). According to the results of cellular uptake, CCP binding to liposome was conducive to liposome absorption into the cell.

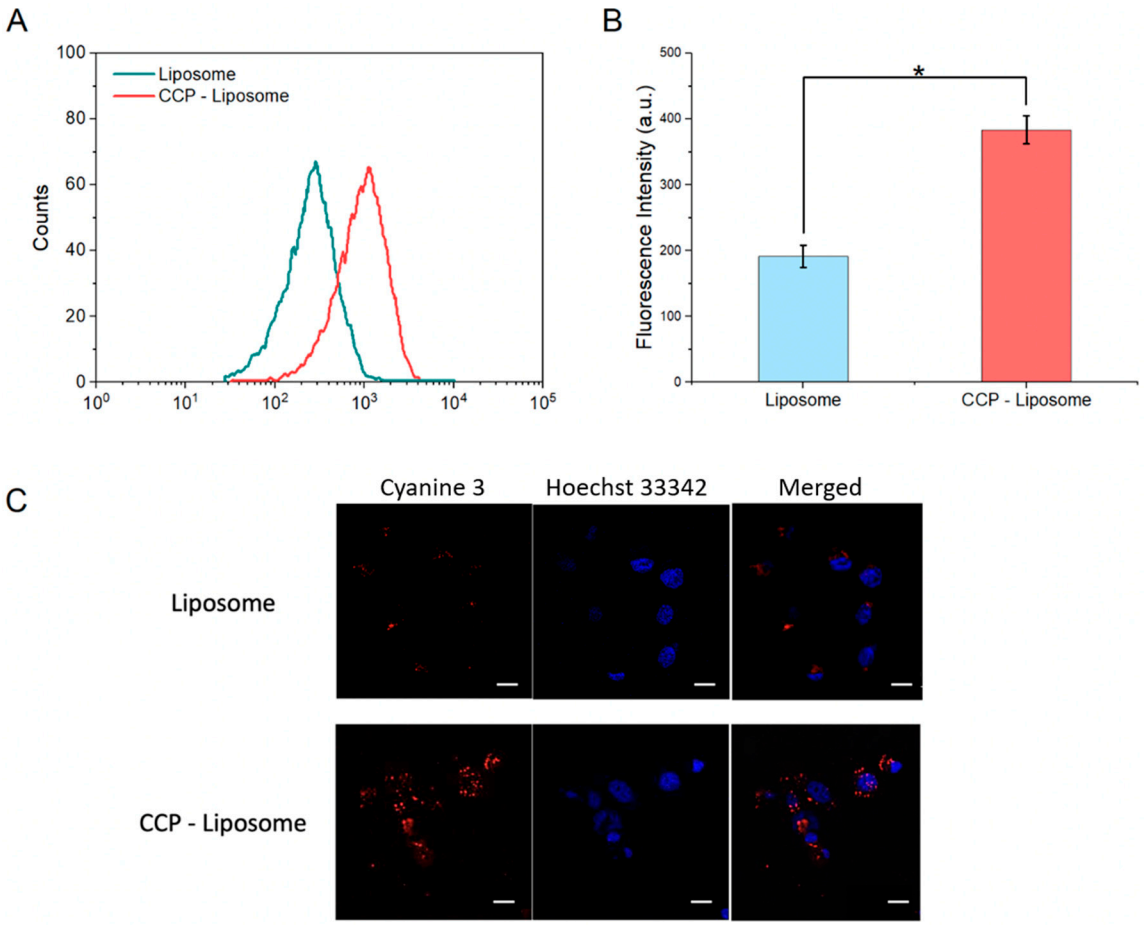

Figure 5. Cellular uptake of liposome and CCP–liposome on HepG2 cell. (**A**) The peak fluorescence of liposome and CCP–liposome shown on the flow cytometry histogram. (**B**) Fluorescence intensity in HepG2 cells treated with liposome and CCP–liposome was quantified. The values are presented as the mean ± standard deviation ($n = 5$, * $p < 0.05$ considered as statistical difference). (**C**) Confocal laser scanning microscopy (CLSM) was utilized to monitor the intracellular mobility of liposome and CCP–liposome. Cyanine 3 (red) was utilized for visualization, while the cell nuclei were stained with Hoechst 33342 (blue). Scale bars indicate 20 μm.

The intracellular distribution of CCP–liposomes was studied using confocal laser scanning microscopy to validate the improved endosomal escape abilities of the charge-conversion liposomes. This study made use of cyanine-3-labeled liposomes, as seen in Figure 6A. Upon release of the CCP–liposomes from acidic vesicles within the cells, the fluorescence signal transitions from yellow to red. In Figure 6A, CCP–liposomes could escape from endosomes even only after 3 h and almost 80% of CCP–liposomes escaped after 24 h. The confocal images also showed cells changed from the yellow color to almost red inside the cell after 24 h. Figure 6B summarizes the quantitative assessments of the CLSM images. As a result, the co-localization of pDNA with PAsp(DET-Aco) in the CLSM pictures should be identified as yellow. At 4 h, the yellow pixels were clearly visible inside

the cells, suggesting CCP–liposome absorption into cells in their intact state. The yellow pixels diminished with time, but the red pixels rose. The rate of liposome co-localization with PAsp(DET-Cit)–Toc was estimated by counting the yellow and red pixels as follows:

$$\text{Co-localization rate} = \frac{number\ of\ yellow\ pixels}{number\ of\ yellow\ and\ red\ pixels}$$

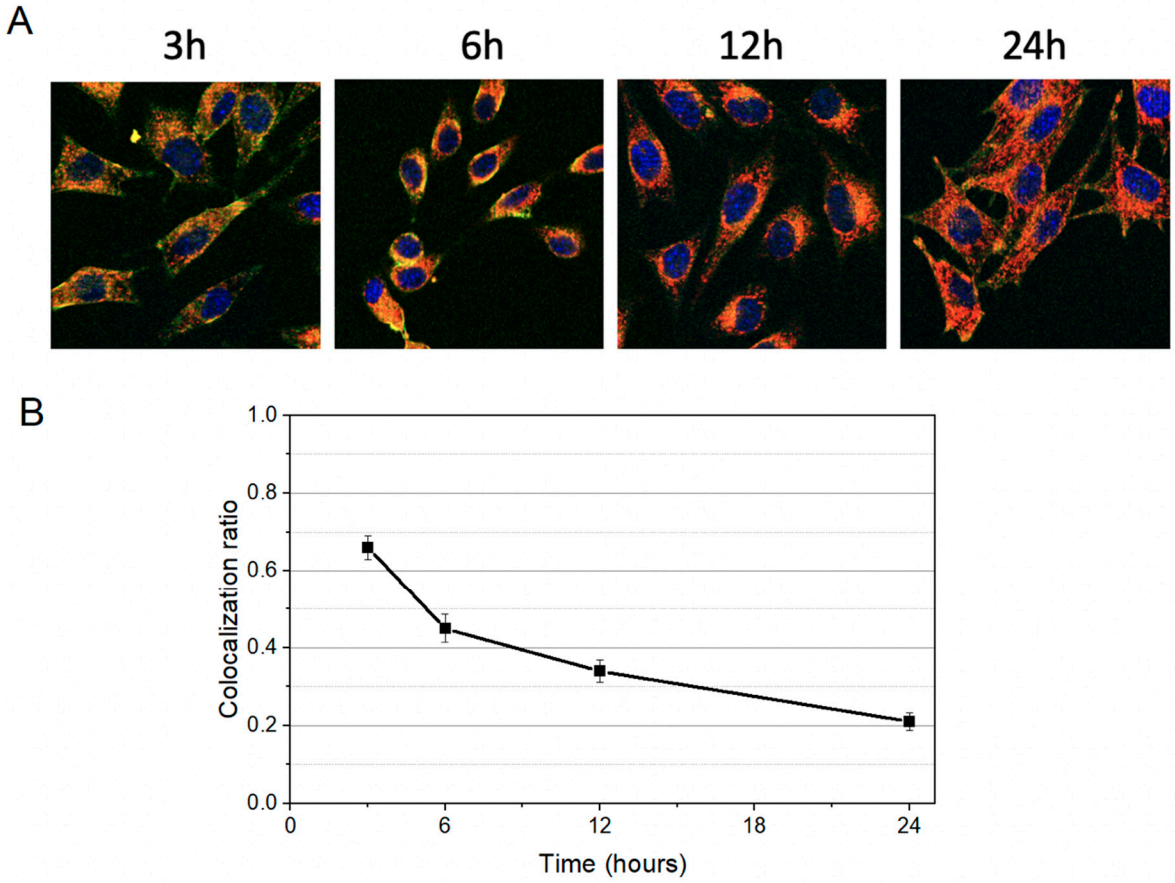

Figure 6. CCP–liposome endosomal escape in a HepG2 cell. (**A**). The color cyanine 3 (red) was utilized. Hoechst 33342 (blue) was used to stain the cell nuclei, while LysoTracker Green (green) was used to stain the late endosome and lysosome. (**B**) Quantitative investigation of CCP–Liposome co-localization at each time point of CLSM observation. Scale bars represent 20 μm.

The quantitative result in Figure 6B clearly showed a steady decline in the co-location rate of liposome with PAsp(DET-Cit)–Toc (CCP–liposome) over time. This finding implies that PAsp(DET-Cit)–Toc internalized with liposomes might revert to PAsp(DET) in acidic endosomal compartments. Eventually, regenerated PAsp(DET) in di-protonated form is expected to be released from the polyplexes, probably by affecting the integrity of the endosomal membrane, as described in prior research [37]. Compared with the study of Kingshuk Dutta et al., only the charge-converting pAsp(DET) polyplexes showed efficient endosomal escape after 24 h and reported releasing ≈80% of encapsulated particles [38].

3.5. In Vitro Cytotoxicity

The cytotoxicity of α–mangostin-loaded CCP–liposome was measured and compared to α–mangostin-loaded-liposome and α–mangostin only. The cells were exposed to active compounds and polymer products for 4 h in different buffer solutions of pH values 5.0, 6.6, and 7.4. MTT assay showed the results in Figure 7. After 4 h of treatment, the cell ability of α–mangostin-loaded-CCP–liposomes incubated in pH 5.0 buffer solutions reduced much more than that incubated in pH 7.4, 6.6 buffer solutions and was close

to free α–mangostin (Figure 7A). In addition, these samples were continued to examine in time course experiment (24–96 h culture). Blank liposomes had no toxicity to cancer cells. α–mangostin-loaded liposomes had less effective on HepG2 cells than α–mangostin only in 24 h treatment, but after 48 h, α–mangostin-loaded liposomes released more α–mangostin inside cells and caused more cytotoxic (Figure 7B). α–mangostin-loaded CCP–liposomes presented the most cytotoxicity compared to the other group. This result proved that α–mangostin-loaded CCP–liposome delivered more effectively α–mangostin into the cell and prevented the degradation of α–mangostin inside cells, especially endosomal degradation. In the Lei Jiang et al. study, the introduction of paclitaxel (PTX) into charge conversional liposomes resulted in enhanced cytotoxicity in both lung cancer A549 cells and drug-resistant lung cancer A549/Taxol cells, surpassing the effects observed with free PTX and PTX-loaded traditional liposomes [39].

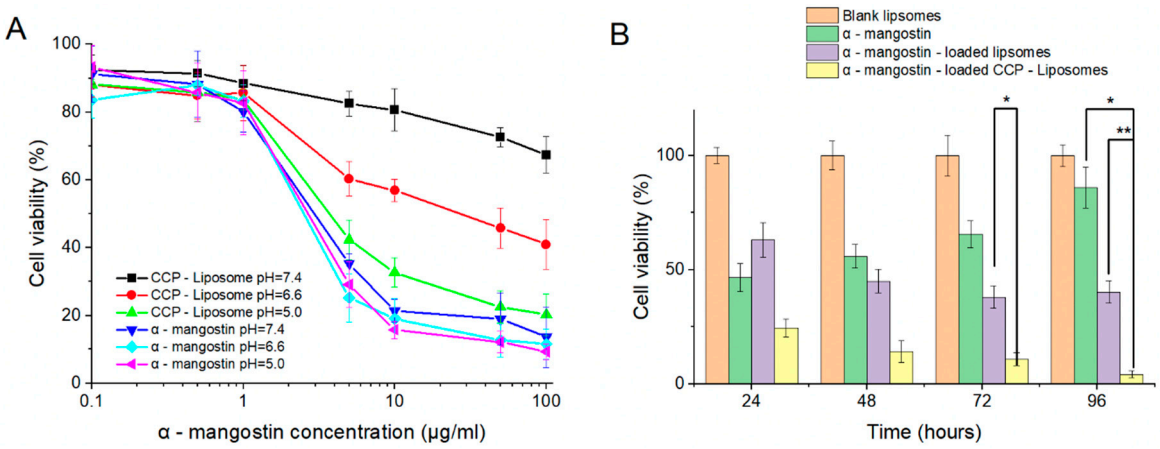

Figure 7. Cytotoxicity effects of α–mangostin, α–mangostin-loaded CCP–Liposome on $HepG_2$ cells in (**A**) 4 h of culture with different pH buffer and α–mangostin concentration from 0.1 to 100 μg/mL and (**B**) from 24 to 96 h of culture with α–mangostin concentration of 5 μg/mL. Data are presented as the mean ± SD (n = 3, * $p < 0.05$; ** $p < 0.01$ considered as statistical difference).

4. Conclusions

In this research, we are continuing to modify and improve the α–mangostin-based-liposome-delivery system for obtaining the ideal therapeutic effects of α–mangostin. It was effectively packaged with liposomes and showed effective cytotoxicity against HepG2 cells in our prior work [20]. However, liposomes face endosomal degradation and then decrease drug delivery efficiency. To circumvent this constraint, PAsp(DET-Cit)–Toc, which has a charge-conversion property, was merged into liposomes to create the CCP–liposome, which has improved drug transport efficiency toward HepG2 cells. DLS analysis revealed that this CCP–liposome drug loading yield reached the highest encapsulation efficiency of 17.4% with 150 μg/mL of α–mangostin. In an acidic environment, the CCP–liposome swelled and erupted, releasing the encapsulated drug into the cytoplasm that reached 50% after 12 h. Furthermore, confocal pictures increased the involvement of PAsp(DET-Cit)–Toc to the endosomal escape of CCP–Liposomes via the charge-conversion process. Furthermore, α–mangostin-loaded CCP–liposomes presented the worst cell viability of 7% after 96 h compared to other groups in the cytotoxicity test. The terminal group of PAsp(DET-Cit)–Toc can be used to conjugate multiple ligands and offer active targeted drug delivery in the future.

Author Contributions: D.T.N. and T.Q.T. conceptualization. T.T.K.P. and D.T.N. conceived and designed the experiments, performed the experiments, analyzed the data, contributed reagents/materials/analysis tools, prepared figures and/or tables, authored or reviewed drafts of the paper. T.T.K.P., D.T.N., L.P.N., U.T.P., H.H.N., X.T.N., T.V.N. and L.A.D. performed the experiments, analyzed the data. D.T.N., T.T.K.P. and H.N.L. contributed to do experiments and revised the manuscript. D.T.N.P.

contributed to writing-review and editing. All authors have read and agreed to the published version of the manuscript.

Funding: This research is funded by Graduate University of Science and Technology under grant number GUST.STS.ĐT2020-SH11.

Data Availability Statement: Not applicable.

Acknowledgments: The authors gratefully acknowledge the support from the Vietnam Academy of Science and Technology.

Conflicts of Interest: The authors declare no conflict of interest.

References

1. Tsai, S.Y.; Chung, P.C.; Owaga, E.E.; Tsai, I.J.; Wang, P.Y.; Tsai, J.I.; Yeh, T.S.; Hsieh, R.H. Alpha-mangostin from mangosteen (*Garcinia mangostana Linn*.) pericarp extract reduces high fat-diet induced hepatic steatosis in rats by regulating mitochondria function and apoptosis. *Nutr. Metab.* **2016**, *13*, 88. [CrossRef]
2. Kritsanawong, S.; Innajak, S.; Imoto, M.; Watanapokasin, R. Antiproliferative and apoptosis induction of alpha-mangostin in T47D breast cancer cells. *Int. J. Oncol.* **2016**, *48*, 2155–2165. [CrossRef]
3. Ovalle-Magallanes, B.; Eugenio-Perez, D.; Pedraza-Chaverri, J. Medicinal properties of mangosteen (*Garcinia mangostana* L.): A comprehensive update. *Food Chem. Toxicol.* **2017**, *109*, 102–122. [CrossRef]
4. Shan, T.; Ma, Q.; Guo, K.; Liu, J.; Li, W.; Wang, F.; Wu, E. Xanthones from mangosteen extracts as natural chemopreventive agents: Potential anticancer drugs. *Curr. Mol. Med.* **2011**, *11*, 666–677. [CrossRef]
5. Hung, S.H.; Shen, K.H.; Wu, C.H.; Liu, C.L.; Shih, Y.W. Alpha-mangostin suppresses PC-3 human prostate carcinoma cell metastasis by inhibiting matrix metalloproteinase-2/9 and urokinase-plasminogen expression through the JNK signaling pathway. *J. Agric. Food Chem.* **2009**, *57*, 1291–1298. [CrossRef] [PubMed]
6. Shih, Y.W.; Chien, S.T.; Chen, P.S.; Lee, J.H.; Wu, S.H.; Yin, L.T. Alpha-mangostin suppresses phorbol 12-myristate 13-acetate-induced MMP-2/MMP-9 expressions via alphavbeta3 integrin/FAK/ERK and NF-kappaB signaling pathway in human lung adenocarcinoma A549 cells. *Cell Biochem. Biophys.* **2010**, *58*, 31–44. [CrossRef] [PubMed]
7. Phan, T.K.T.; Shahbazzadeh, F.; Pham, T.T.H.; Kihara, T. Alpha-mangostin inhibits the migration and invasion of A549 lung cancer cells. *PeerJ* **2018**, *6*, e5027. [CrossRef] [PubMed]
8. Li, P.; Tian, W.; Ma, X. Alpha-mangostin inhibits intracellular fatty acid synthase and induces apoptosis in breast cancer cells. *Mol. Cancer* **2014**, *13*, 138. [CrossRef]
9. Li, L.; Brunner, I.; Han, A.R.; Hamburger, M.; Kinghorn, A.D.; Frye, R.; Butterweck, V. Pharmacokinetics of alpha-mangostin in rats after intravenous and oral application. *Mol. Nutr. Food Res.* **2011**, *55* (Suppl. S1), S67–S74. [CrossRef]
10. Wathoni, N.; Rusdin, A.; Motoyama, K.; Joni, I.M.; Lesmana, R.; Muchtaridi, M. Nanoparticle Drug Delivery Systems for alpha-Mangostin. *Nanotechnol. Sci. Appl.* **2020**, *13*, 23–36. [CrossRef] [PubMed]
11. Xu, S.; Olenyuk, B.Z.; Okamoto, C.T.; Hamm-Alvarez, S.F. Targeting receptor-mediated endocytotic pathways with nanoparticles: Rationale and advances. *Adv. Drug Deliv. Rev.* **2013**, *65*, 121–138. [CrossRef] [PubMed]
12. Cerqueira, B.B.; Lasham, A.; Shelling, A.N.; Al-Kassas, R. Nanoparticle therapeutics: Technologies and methods for overcoming cancer. *Eur. J. Pharm. Biopharm.* **2015**, *97*, 140–151. [CrossRef]
13. Sercombe, L.; Veerati, T.; Moheimani, F.; Wu, S.Y.; Sood, A.K.; Hua, S. Advances and Challenges of Liposome Assisted Drug Delivery. *Front. Pharmacol.* **2015**, *6*, 286. [CrossRef] [PubMed]
14. Daraee, H.; Etemadi, A.; Kouhi, M.; Alimirzalu, S.; Akbarzadeh, A. Application of liposomes in medicine and drug delivery. *Artif. Cells Nanomed. Biotechnol.* **2016**, *44*, 381–391. [CrossRef]
15. Hua, S.; Wu, S.Y. The use of lipid-based nanocarriers for targeted pain therapies. *Front. Pharmacol.* **2013**, *4*, 143. [CrossRef]
16. Ding, B.S.; Dziubla, T.; Shuvaev, V.V.; Muro, S.; Muzykantov, V.R. Advanced drug delivery systems that target the vascular endothelium. *Mol. Interv.* **2006**, *6*, 98–112. [CrossRef]
17. Metselaar, J.M.; Storm, G. Liposomes in the treatment of inflammatory disorders. *Expert Opin. Drug Deliv.* **2005**, *2*, 465–476. [CrossRef] [PubMed]
18. Das, S.S.; Hussain, A.; Verma, P.R.P.; Imam, S.S.; Altamimi, M.A.; Alshehri, S.; Singh, S.K. Recent Advances in Liposomal Drug Delivery System of Quercetin for Cancer Targeting: A Mechanistic Approach. *Curr. Drug Deliv.* **2020**, *17*, 845–860. [CrossRef]
19. Li, M.; Du, C.; Guo, N.; Teng, Y.; Meng, X.; Sun, H.; Li, S.; Yu, P.; Galons, H. Composition design and medical application of liposomes. *Eur. J. Med. Chem.* **2019**, *164*, 640–653. [CrossRef]
20. Trang Phan, T.K.; Tran, T.Q.; Nguyen Pham, D.T.; Nguyen, D.T. Characterization, Release Pattern, and Cytotoxicity of Liposomes Loaded With α-Mangostin Isolated From Pericarp of Mangosteen (*Garcinia mangostana* L.). *Natural. Prod. Commun.* **2020**, *15*, 1934578X20974559. [CrossRef]
21. Rommasi, F.; Esfandiari, N. Liposomal Nanomedicine: Applications for Drug Delivery in Cancer Therapy. *Nanoscale Res. Lett.* **2021**, *16*, 95. [CrossRef] [PubMed]
22. Fanciullino, R.; Ciccolini, J. Liposome-encapsulated anticancer drugs: Still waiting for the magic bullet? *Curr. Med. Chem.* **2009**, *16*, 4361–4371. [CrossRef] [PubMed]

23. Torchilin, V. Tumor delivery of macromolecular drugs based on the EPR effect. *Adv. Drug Deliv. Rev.* **2011**, *63*, 131–135. [CrossRef]
24. Bozzuto, G.; Molinari, A. Liposomes as nanomedical devices. *Int. J. Nanomed.* **2015**, *10*, 975–999. [CrossRef] [PubMed]
25. Canton, I.; Battaglia, G. Endocytosis at the nanoscale. *Chem. Soc. Rev.* **2012**, *41*, 2718–2739. [CrossRef]
26. Bae, Y.; Nishiyama, N.; Fukushima, S.; Koyama, H.; Yasuhiro, M.; Kataoka, K. Preparation and biological characterization of polymeric micelle drug carriers with intracellular pH-triggered drug release property: Tumor permeability, controlled subcellular drug distribution, and enhanced in vivo antitumor efficacy. *Bioconjug. Chem.* **2005**, *16*, 122–130. [CrossRef]
27. Huang, H.; Li, Y.; Sa, Z.; Sun, Y.; Wang, Y.; Wang, J. A smart drug delivery system from charge-conversion polymer-drug conjugate for enhancing tumor therapy and tunable drug release. *Macromol. Biosci.* **2014**, *14*, 485–490. [CrossRef]
28. Sun, H.; Guo, B.; Li, X.; Cheng, R.; Meng, F.; Liu, H.; Zhong, Z. Shell-sheddable micelles based on dextran-SS-poly(epsilon-caprolactone) diblock copolymer for efficient intracellular release of doxorubicin. *Biomacromolecules* **2010**, *11*, 848–854. [CrossRef]
29. Gallon, E.; Matini, T.; Sasso, L.; Mantovani, G.; Arminan de Benito, A.; Sanchis, J.; Caliceti, P.; Alexander, C.; Vicent, M.J.; Salmaso, S. Triblock Copolymer Nanovesicles for pH-Responsive Targeted Delivery and Controlled Release of siRNA to Cancer Cells. *Biomacromolecules* **2015**, *16*, 1924–1937. [CrossRef]
30. Selby, L.I.; Cortez-Jugo, C.M.; Such, G.K.; Johnston, A.P.R. Nanoescapology: Progress toward understanding the endosomal escape of polymeric nanoparticles. *Wiley Interdiscip. Rev. Nanomed. Nanobiotechnol.* **2017**, *9*, e1452. [CrossRef]
31. Harada, A.; Kataoka, K. Formation of Polyion Complex Micelles in an Aqueous Milieu from a Pair of Oppositely-Charged Block Copolymers with Poly(ethylene glycol) Segments. *Macromolecules* **1995**, *25*, 5294–5299. [CrossRef]
32. Tang, J.; He, J.; Yang, C.; Mao, Y.; Hu, T.; Zhang, L.; Cao, H.; Tong, A.; Song, X.; He, G.; et al. Antitumor Effects of MsurvivinT34A–CaPi Complex-Embedded PLGA Nanoparticles in Combination with Doxil in Mice. *J. Nanopart. Res.* **2014**, *16*, 2682. [CrossRef]
33. Lee, Y.; Fukushima, S.; Bae, Y.; Hiki, S.; Ishii, T.; Kataoka, K. A protein nanocarrier from charge-conversion polymer in response to endosomal pH. *J. Am. Chem. Soc.* **2007**, *129*, 5362–5363. [CrossRef]
34. Bae, Y.; Jang, W.D.; Nishiyama, N.; Fukushima, S.; Kataoka, K. Multifunctional polymeric micelles with folate-mediated cancer cell targeting and pH-triggered drug releasing properties for active intracellular drug delivery. *Mol. Biosyst.* **2005**, *1*, 242–250. [CrossRef]
35. Koide, A.; Kishimura, A.; Osada, K.; Jang, W.D.; Yamasaki, Y.; Kataoka, K. Semipermeable polymer vesicle (PICsome) self-assembled in aqueous medium from a pair of oppositely charged block copolymers: Physiologically stable micro-/nanocontainers of water-soluble macromolecules. *J. Am. Chem. Soc.* **2006**, *128*, 5988–5989. [CrossRef]
36. Fan, J.; Borguet, Y.P.; Su, L.; Nguyen, T.P.; Wang, H.; He, X.; Zou, J.; Wooley, K.L. Two-Dimensional Controlled Syntheses of Polypeptide Molecular Brushes via N-Carboxyanhydride Ring-Opening Polymerization and Ring-Opening Metathesis Polymerization. *ACS Macro Lett.* **2017**, *6*, 1031–1035. [CrossRef]
37. Sanjoh, M.; Hiki, S.; Lee, Y.; Oba, M.; Miyata, K.; Ishii, T.; Kataoka, K. pDNA/poly(L-lysine) Polyplexes Functionalized with a pH-Sensitive Charge-Conversional Poly(aspartamide) Derivative for Controlled Gene Delivery to Human Umbilical Vein Endothelial Cells. *Macromol. Rapid Commun.* **2010**, *31*, 1181–1186. [CrossRef]
38. Dutta, K.; Das, R.; Medeiros, J.; Kanjilal, P.; Thayumanavan, S. Charge-Conversion Strategies for Nucleic Acid Delivery. *Adv. Funct. Mater.* **2021**, *31*, 2011103. [CrossRef] [PubMed]
39. Jiang, L.; Li, L.; He, X.; Yi, Q.; He, B.; Cao, J.; Pan, W.; Gu, Z. Overcoming drug-resistant lung cancer by paclitaxel loaded dual-functional liposomes with mitochondria targeting and pH-response. *Biomaterials* **2015**, *52*, 126–139. [CrossRef]